




Characterization of NiO based ceramics modified with Y₂O₃/BiSbO₃ for application of NTC thermistors

Dicheng Peng¹, Zhicheng Li¹, Linling Huang¹, Chang You¹, Hanxiao Wang¹, and Hong Zhang^{1,*} 

¹ School of Materials Science and Engineering, Central South University, Changsha 410083, China

Received: 17 February 2022

Accepted: 14 March 2022

Published online:

24 March 2022

© The Author(s), under exclusive licence to Springer Science+Business Media, LLC, part of Springer Nature 2022

ABSTRACT

Facing the development of electronic information technology, measurement and control technology towards diversity and higher precision, it is interesting to design and fabricate thermistors with effect of negative temperature coefficient (NTC) of resistivity with adjustable room temperature resistivity (ρ_{25}), high thermal sensitivity and electrical stability. Here, NiO-based ceramics doped with Y₂O₃ and modified by BiSbO₃ were prepared by solid state reaction method. Phase component, microstructure, electrical properties and aging performances of the prepared ceramics were investigated. The prepared ceramics have main phase with cubic rock salt structure and present typical NTC characteristics. Doping with Y₂O₃ and BiSbO₃ can effectively adjust the ρ_{25} of NiO based ceramics, which show high temperature sensitivity with NTC material constants ($B_{25/85}$ value) larger than 5200 K. The introduction of BiSbO₃ into Y-doped NiO ceramics can effectively enhance the electrical stability. The aging-induced resistance change rate of the Y-doped NiO ceramics is -5.9% after aging for 800 h (treated at 150 °C in air), while the Y-doped NiO ceramics modified with 2 wt% of BiSbO₃ have only 0.21% of resistance change rate after aging treatment. The aging mechanism was analyzed by X-ray photoelectron spectroscopies of the ceramics before and after aging.

1 Introduction

Negative temperature coefficient (NTC) thermistors have the feature that their resistivities decrease with the temperature increasing. They are widely used in fields for measurement and control of temperature, suppression of surge current, temperature compensation and protection from overheating, etc. [1–5]. The traditional NTC thermistors are normally made

of spinel structure compounds consisting of transition metal oxides such as manganates [6–10]. Much work have been performed to modify the electrical properties using various methods such as doping with heterovalent cations, forming hybrid structures and manipulating preparation process [11–13]. In recent years, the NTC thermistors based on single cation-based oxide such as NiO, ZnO, SnO₂ or CuO have also drawn much attention [14–17], because

Address correspondence to E-mail: hzhang@csu.edu.cn

they have the advantage of adjustable resistivity and thermosensitivity by suitable element doping [15, 16, 18]. For instances, Yang et al. reported that the NiO-based ceramics achieved room temperature resistivity (ρ_{25}) ranging from 47.94 Ω cm to 1.024 M Ω cm and contained NTC material constants ($B_{25/85}$ values) from 2582 to 8019 K by doping with various concentrations of B^{3+} and Na^+ cations [14]. Ouyang et al. reported that SnO_2 based ceramics showed typical NTC characteristics in a wide temperature range of -50 to 300 $^{\circ}C$, and doping with Sb- and Zr^{4+} -ions can effectively adjust ρ_{25} and $B_{25/85}$ values [19].

Besides ρ_{25} and $B_{25/85}$, electrical stability is also a key performance for the application of NTC thermistors. One of general methods to characterize electrical stability is measuring the change rate of resistance ($\Delta R/R_0$) of a NTC thermistor during aging under a certain temperature environment. The aging induced $\Delta R/R_0$ might result from various mechanisms such as ionic rearrangement, oxidation or reduction of elements [15, 20–22]. Battault et al. monitored the aging effect in $Mn_{3-x}Fe_xO_4$ ($0 \leq x \leq 1.51$) via Mössbauer spectroscopy and found that the redistribution of Fe^{3+} ions between the tetrahedral and octahedral sites induced the resistance increase during aging process [21]. Ma et al. studied the effect of Zn^{2+} -ion doping on the aging stability of $Ni_{0.6}Cu_{0.5}Zn_xMn_{1.9-x}O_4$ spinel-type ceramics, and found that Zn dopant could significantly reduce $\Delta R/R_0$ of ceramics from 10.2% ($x = 0$) to 0.02% ($x = 0.75$). These are owe to that Zn^{2+} ions could restrain the redistribution of Cu^{2+} ions during aging process [23]. Recently, aging characteristics of the NTC thermistors based on single cation oxides have also been reported. For example, Jiang et al. reported that $Sn_{0.95}Sb_{0.05}O_2$ -based NTC ceramics showed excellent electrical stability for that the introduction of MnO_2 suppressed the oxidation of Sb^{3+} ions [16]. Gao et al. suggested the space charge distribution and interface barrier model for the aging mechanism of $(Zn_{0.4}Ni_{0.6})_{1-x}Na_xO$ thermistors [24]. During aging process, oxygen molecules are adsorbed on ceramic surface and then capture electrons from the ceramic surface and/or interface, the hole concentration in ceramic decreases accordingly in order to maintain the electrical neutrality of the space-charge layer, resulting in the increase of interface barrier and ceramic resistivity. While, in the Bi-modified $(Zn_{0.4}Ni_{0.6})_{1-x}Na_xO$ ceramics, the adsorbed oxygen easily captures

electrons from the Bi-rich regions, regulated the interface barrier and bulk resistivity, and improved the aging stability of ceramics.

Although lots of work on NTC thermistors based on single cation oxide have been reported, there has been few report on the aging performance of NiO-based ceramics so far. The electrical stability is significant for the practical applications as electronic components. In this work, NiO-based ceramics doped with Y_2O_3 or codoped with $Y_2O_3/BiSbO_3$ were prepared by the conventional solid state method, and their electrical properties and aging stability were investigated. The results show that the prepared ceramics have typical NTC effects, and the ρ_{25} can be adjusted from 1143 to 19,188 Ω cm by changing the dopant content, while the material constants $B_{25/85}$ are always above 5200 K. $Y_2O_3/BiSbO_3$ modified NiO ceramic can achieve high electrical stability with $\Delta R/R_0 = 0.21\%$ after aging at 150 $^{\circ}C$ for 800 h in air.

2 Experimental

NiO-based ceramics were prepared by the conventional solid state reaction method. Nickel carbonate ($NiCO_3 \cdot 2Ni(OH)_2 \cdot 4H_2O$, $\geq 99.0\%$, Xilong Scientific, China) and yttrium oxide (Y_2O_3 , $\geq 99.0\%$, Tianjin Kemiou Chemical, China), bismuth oxide (Bi_2O_3 , $\geq 99.9\%$, Changsha Yaguang Trade Co., Ltd, China), antimony trioxide (Sb_2O_5 , $\geq 99.0\%$, Sinopharm Chemical Reagent Co, China) were used as raw materials without any further purification. The $BiSbO_3$ (denoted as BSO) compound was prepared with Bi_2O_3 and Sb_2O_5 in mole ratio of 1:1. Raw materials were accurately weighed according to nominal formulas $Ni_{1-x}Y_xO$ ($x = 0, 0.005, 0.01, 0.015, 0.02, 0.03$, denoted as $xNYO$) to prepare the Y-doped NiO ceramics. The raw materials were mixed by thoroughly grinding and then calcined at 900 $^{\circ}C$ for 5 h in air. Some of the as-calcined powders were granulated with proper amount of ethylene glycol as binder. The other calcined powders were mixed with various contents of BSO according to the compositions of $Ni_{0.99}Y_{0.01}O-y\%$ BSO ($y = 1, 2, 4, 6$, weight ratio, denoted as $0.01NYO-yBSO$), and then were granulated with proper amount of ethylene glycol as binder. Then the granulated powders were pressed into cylindrical pellets with diameter of 12 mm and thickness of about 3 mm. Green pellets were sintered at 1300 – 1380 $^{\circ}C$ for 1 h in air. Both opposite surface

sides of as-sintered ceramics were polished and coated with silver paste followed by heating in a tube furnace at 600 °C for 5 min to obtain ohmic-contact electrodes.

To determine the phase component, the ceramics were characterized using X-ray diffractometer (XRD, Rigaku D/max 2500, Japan. Cu Ka-ray, $\lambda = 0.154056$ nm) with diffraction angle (2θ) in the range of 20°–90° at a scanning rate of 8°/min. Microstructures of ceramics was characterized by field emission scanning electron microscopy (SEM, JMS-7900 F). Samples for SEM analysis, the ceramics were broken into pieces and cleaned by ultrasonic treatment in advance, and the fracture surfaces were observed. The elemental distributions in ceramics was characterized by energy dispersive X-ray spectroscopy (EDS, Oxford Ultim Max 65) attached to SEM. Elemental valence states in the samples were analyzed using X-ray photoelectron spectroscopy (XPS, K-alpha 1063, UK) recorded under Al Ka radiation ($h_m = 1486.6$ eV). The relative density (D_r) of each sample was tested by Archimedes method and calculated according to equation of $D_r = D_m/D_i$, where D_m is measured density and D_i is theoretical density of NiO crystal.

The resistance–temperature (R – T) characteristics of ceramics were characterized by a resistance–temperature test system (ZWX-C, China) under direct-current (DC) condition in temperature range between 25 and 250 °C. The resistivity (ρ) was calculated by equation of $\rho = RS/L$, where R is measured resistance, S is area of electrodes, and L is sample thickness. The alternating current (AC) complex impedance spectra, measured at temperatures from 25 to 60 °C and in frequency range from 1 Hz to 1 MHz, were measured by electrochemical test system (Gamry Reference 600, USA). Each complex impedance spectroscopy (CIS) was analyzed using Gamry Echem Analyst program. In order to characterize electrical stability, ageing treatment was performed at 150 °C for 800 h in air. The aging induced resistance change rate of each sample was defined by equation $\Delta R/R_0 = (R_1 - R_0)/R_0$, where R_0 and R_1 are resistances before and after aging, respectively, and were measured at room temperature (25 °C).

3 Result and discussion

3.1 Phase component and microstructure

Figure 1 shows XRD patterns of the as-sintered ceramics. The main phase of all samples could be determined to NiO cubic rock-salt structure with a space group of $Fm\bar{3}m$ (225) (Ref. PDF No. 47-1049). (111), (200), (220), (311) and (222) crystal planes of the main phase are indexed. Apart from the main phase, additional three diffraction peaks at 2θ of 29.2°, 33.9° and 48.6° corresponding to (111), (200) and (220) crystal planes of Y_2O_3 (Ref. PDF No. 43-0661) can be determined in 0.03NYO and 0.01NYO-2BSO samples. Only a weak diffraction peak at 29.2° corresponding to (111) plane of Y_2O_3 phase can be observed in 0.01NYO ceramic, which might due to its small amount. These indicate that the solid solubility Y_2O_3 in NiO crystal is small, for the large difference of ionic radii between Y^{3+} -ion (0.090 nm) and Ni^{2+} ion (0.069 nm). While, in XRD pattern of 0.01NYO-6BSO, peaks at 30.0°, 34.8°, 50.1° and 59.6° corresponding to (222), (400), (440) and (622) of $(BiSbY)_2O_4$ phase (Ref. PDF No. 73-1735) were detected. In the 0.01NYO-6BSO ceramic, the second phase $(BiSbY)_2O_4$ instead of Y_2O_3 phase was detected, indicating that Y-ions have dissolved into NiO and $(BiSbY)_2O_4$ phase.

SEM images of fracture surfaces of 0NYO, 0.01NYO and 0.03NYO ceramics are shown in Fig. 2. It can be seen that the grains in all samples are tightly bonded, although some small pores could be

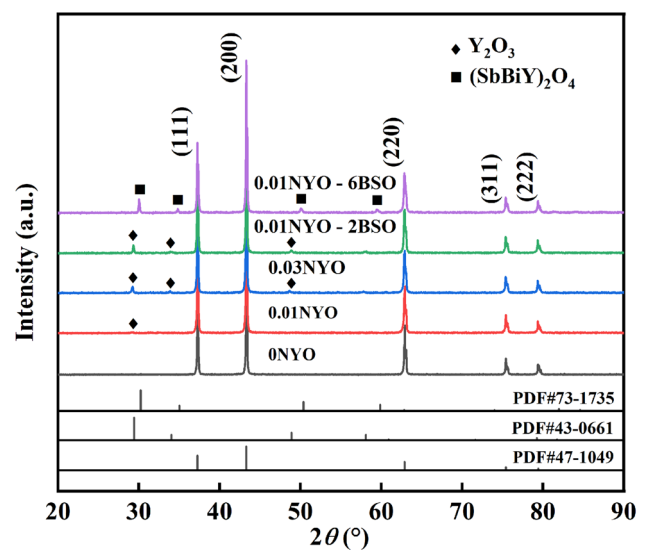


Fig. 1 XRD patterns of the as-sintered NiO-based ceramics

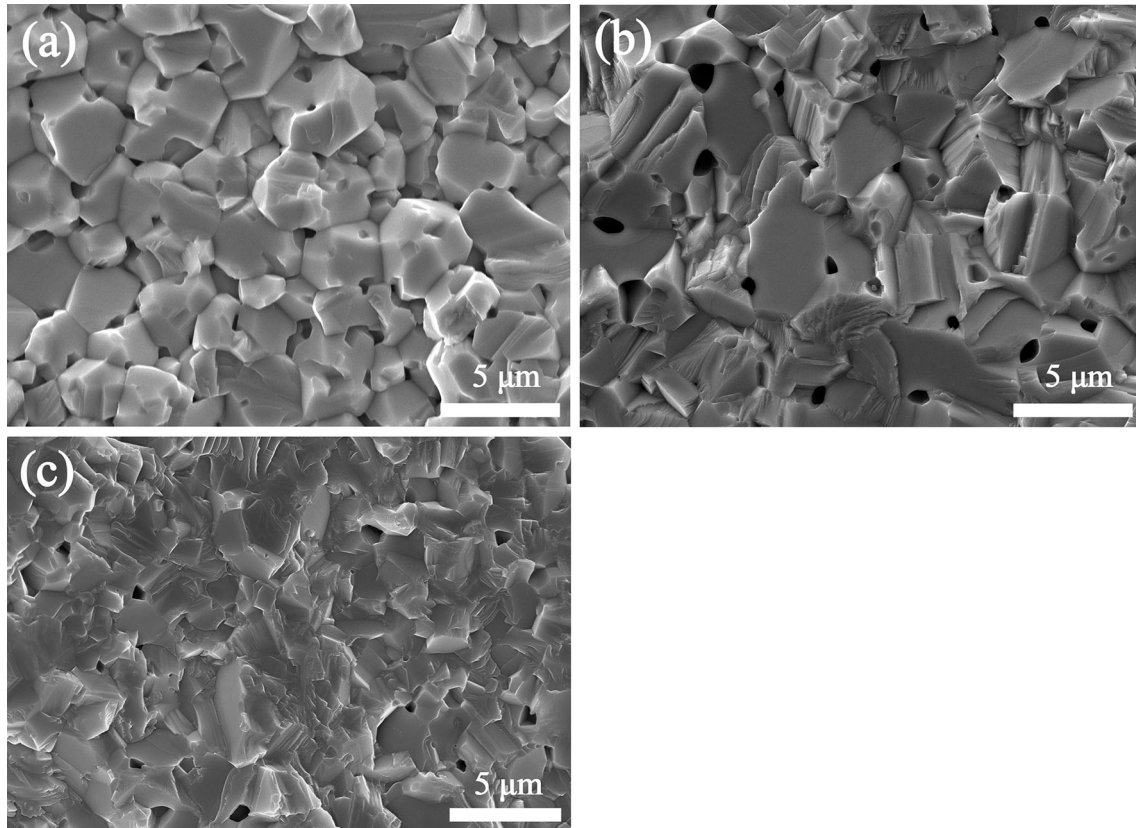


Fig. 2 SEM images of x NYO ceramics with various contents of Y^{3+} -ions, a 0NYO, b 0.01NYO, c 0.03NYO

observed. It is noteworthy that numbers of pore show a decreasing trend with content increasing of Y^{3+} -ions. This can be further confirmed by the measured relative densities. The relative densities of 0NYO, 0.01NYO and 0.03NYO ceramics are 92%, 96% and 98%, respectively. These indicate that the introduction of Y_2O_3 dopant can enhance the sintering ability. This can be explained as following. The Y_2O_3 doping into NiO lattice can make large lattice distortion for that the radius of Y^{3+} -ion (0.090 nm for coordination number of 6) is larger than that of Ni^{2+} ion (0.069 nm), and lead to large locale distortion energy. At the same time, the substitution of Y^{3+} -ion with + 3 valence at Ni^{2+} ion (+ 2 valence) in NiO crystal might induce partially the formation of cationic vacancy, the defect reaction can be described as $Y_2O_3 \xrightarrow{NiO} 2Y'_{Ni} + V''_{Ni} + 3O_O$. The production of lattice distortion energy and existence of lattice defects may improve the mass migration and diffusion, and facilitates the densification of ceramics during sintering.

Figure 3 shows SEM images and corresponding EDS elemental analysis of 0.01NYO and 0.03NYO

ceramics. Figure 3b and c show respectively the distribution mappings of Ni and Y elements in 0.01NYO ceramic. Figure 3e and f are the distribution mappings of Ni and Y elements in 0.03NYO ceramic, respectively. It can be seen that Ni element uniformly distributes throughout both samples. Y element shows aggregation at certain areas, this phenomenon in 0.03NYO ceramic is clearer than that in 0.01NYO ceramic. This is consistent with the XRD analysis as shown in Fig. 1, where obvious diffraction peaks from Y_2O_3 second phase exist in the Y-doped 0.03NYO ceramic, but weak and indistinct diffraction peaks in 0.01NYO which might due to its tiny content.

Figure 4 shows SEM images and EDS analysis of as-sintered 0.01NYO–2BSO and 0.01NYO–6BSO ceramics. Both ceramics have similar microstructure characteristics of uniform grains. At the same time, some granular particles can be seen in both ceramics. Compared with SEM image of 0.01NYO ceramic as shown in Fig. 2b, the 0.01NYO–2BSO ceramic contains two kinds of small particles in the matrix. The two kinds of small particles are sheet plate shape one

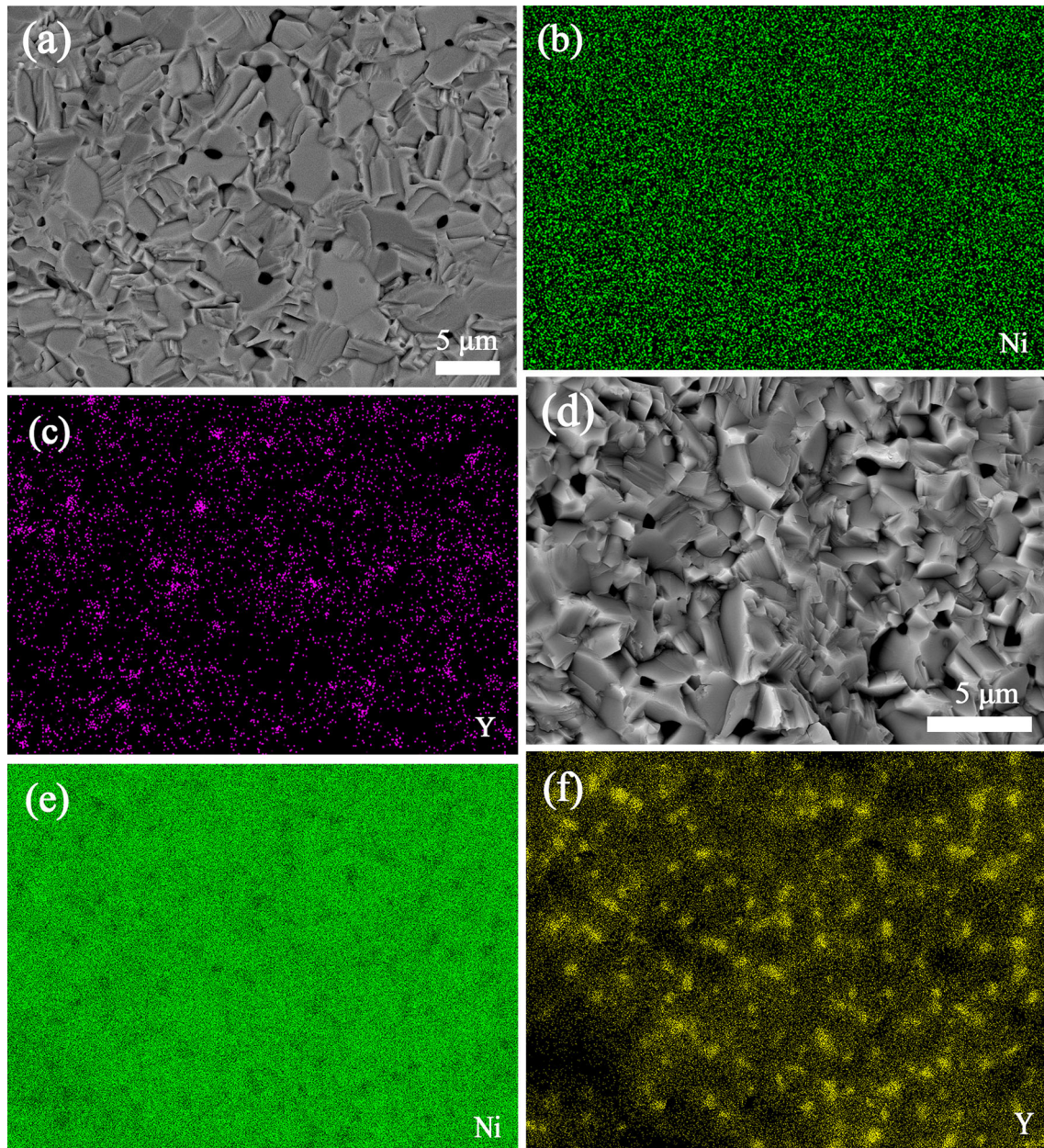


Fig. 3 SEM analysis of 0.01NYO and 0.03NYO ceramics, **a** SEM image of 0.01NYO ceramic (with back scattered electrons), **b** and **c** distribution mapping of Ni and Y elements in 0.01NYO ceramic,

respectively, **d** SEM image of 0.03NYO ceramic, **e** and **f** distribution mapping of Ni and Y elements in 0.03NYO ceramic, respectively

marked (I) and granular shape one marked (II) in Fig. 4a. There are more granular shape particles in 0.01NYO–6BSO ceramic. EDS analysis of the regions (I) and (II) was performed in order to analyze the possible compositions. The results are shown in Fig. 4c and d, and the atomic percentages are shown in Table 1. The results show that both regions have high contents of Y element, while extra Bi and Sb more likely gathering at region (II). It can be deduced

that the sheet plate shape particles might be mainly comprised of Y-cation while the granular shape particles more likely have three kinds of cations of Y-, Bi- and Sb-cations (except Ni, O). Combine with the XRD analysis in Fig. 1, the second phase in 0.01NYO–2BSO ceramic is mainly Y_2O_3 phase (some $(BiSbY)_2O_4$ without XRD diffraction peaks due to its small amount), while second phase in 0.01NYO–6BSO ceramic is mainly $(BiSbY)_2O_4$.

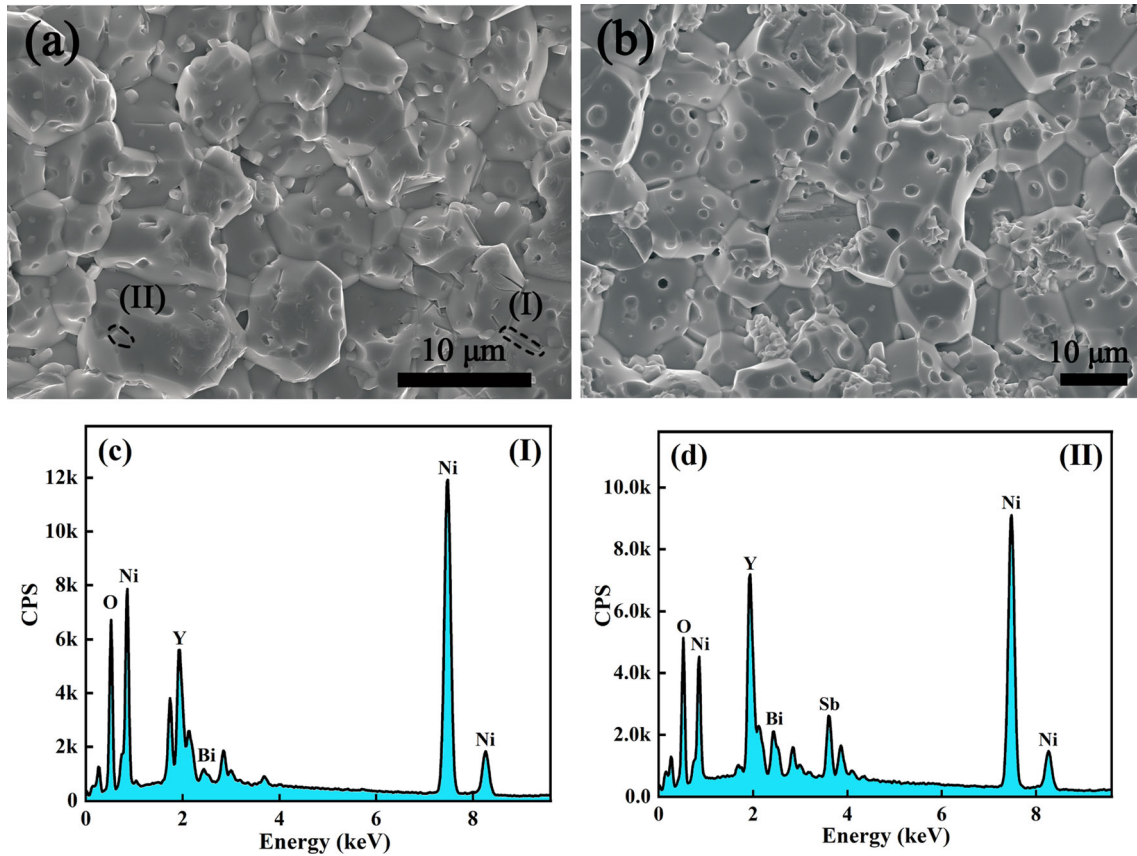


Fig. 4 SEM images of the fracture surface and EDS spectra of 0.01NYO-*y*BSO composite ceramics, **a** SEM image of 0.01NYO-2BSO ceramic, **b** SEM image of 0.01NYO-6BSO ceramic, **c** and **d** EDS spectra of regions (I) and (II) in 0.01NYO-2BSO ceramic, respectively

Table 1 Element content (at%) based on EDS analysis as shown in Fig. 4c and d

	O	Ni	Y	Sb	Bi
Region (I)	54.03	38.98	6.65	0.00	0.34
Region (II)	51.89	34.47	8.09	4.1 9	1.37

Back scattered SEM image of a 0.01NYO-2BSO ceramic and related EDS elemental distributions are shown in Fig. 5. EDS mappings (Fig. 5b-f) shows that Ni and O elements uniformly distribute throughout the ceramic, while Y, Sb and Bi elements are aggregated at certain areas. Combined with the XRD analysis in Fig. 1 and chemical elemental analysis in Fig. 4, one can further confirm that these second phases could be Y₂O₃ and (SbBiY)₂O₄.

3.2 Electrical properties

The influence of doping with Y³⁺-ions and BSO compound on electrical properties of NiO-based ceramics were studied by investigating the temperature dependence of electrical resistivity for ceramics. Figure 6a shows some plots of the relationship between the resistivity (ρ) and absolute temperature (T , in Kelvin) of *x*NYO ceramics. The resistivity decreases with increase of temperature for each ceramic, indicating that all ceramics have typical NTC characteristic. However, the $\ln\rho - 1000/T$ plots do not show single linear relationship over the entire test temperature range, each plot could be comprised of two parts of linear regions with different slopes. According to the Arrhenius law, the $\ln\rho - 1000/T$ plots can be described as Eq. (1).

$$\rho = \rho_0 \exp\left(\frac{\varepsilon E_{a1} + (1 - \varepsilon)E_{a2}}{kT}\right) \tag{1}$$

where, ρ represents resistivity at temperature T , ρ_0 is a constant related to the intrinsic characteristic of

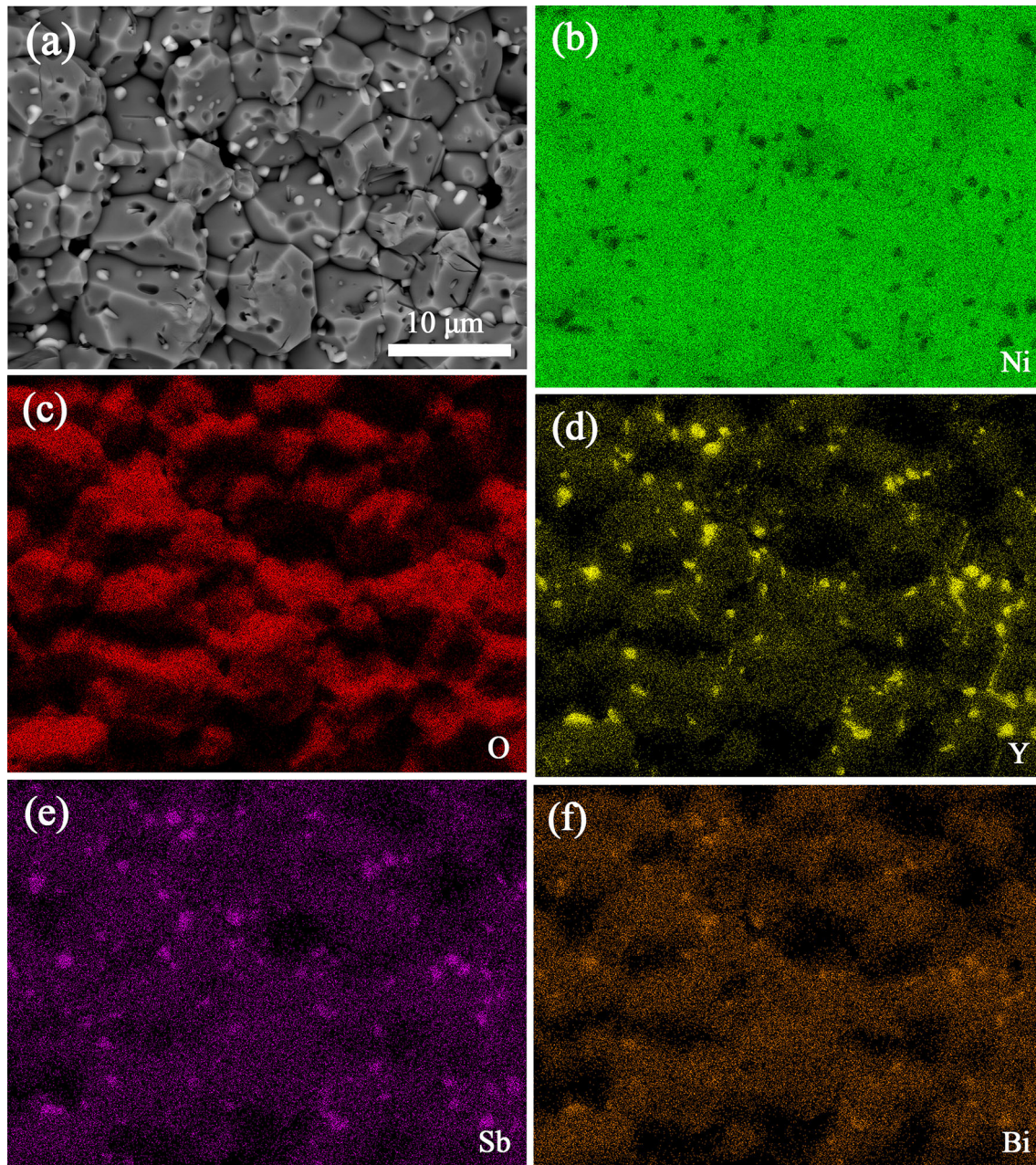


Fig. 5 SEM image and EDS element distribution of 0.01NYO–2BSO ceramic, **a** Back scattered SEM image, **d–f** EDS elemental mappings of Ni, O, Y, Sb and Bi elements, respectively

material, E_{a1} and E_{a2} are activation energies of conduction in the high temperature region and low temperature region, respectively, k is Boltzmann constant, ε ($0 \leq \varepsilon \leq 1$) is a coefficient related to temperature. For 0.01NYO ceramic, E_{a1} and E_{a2} were calculated to be 0.113 eV and 0.457 eV, respectively.

Figure 6b summarizes the Y^{3+} -ion concentration dependence of room temperature resistivity (ρ_{25}) of x NYO ceramics doped with various amount of

Y^{3+} -ions. The ρ_{25} of x NYO ceramics can be adjusted in wide range for various contents of Y^{3+} -ion. When $x \leq 0.015$, $\ln\rho_{25}$ of x NYO ceramics decreases with x increasing. Nevertheless, $\ln\rho_{25}$ increases with x increasing when x is higher than 0.015. These should be mainly caused by the heterovalent doping for the semiconductor NiO. This can be described using defect chemical equation as shown in Eq. (2). One Y^{3+} -ion substitutes into the crystal at Ni^{2+} lattice

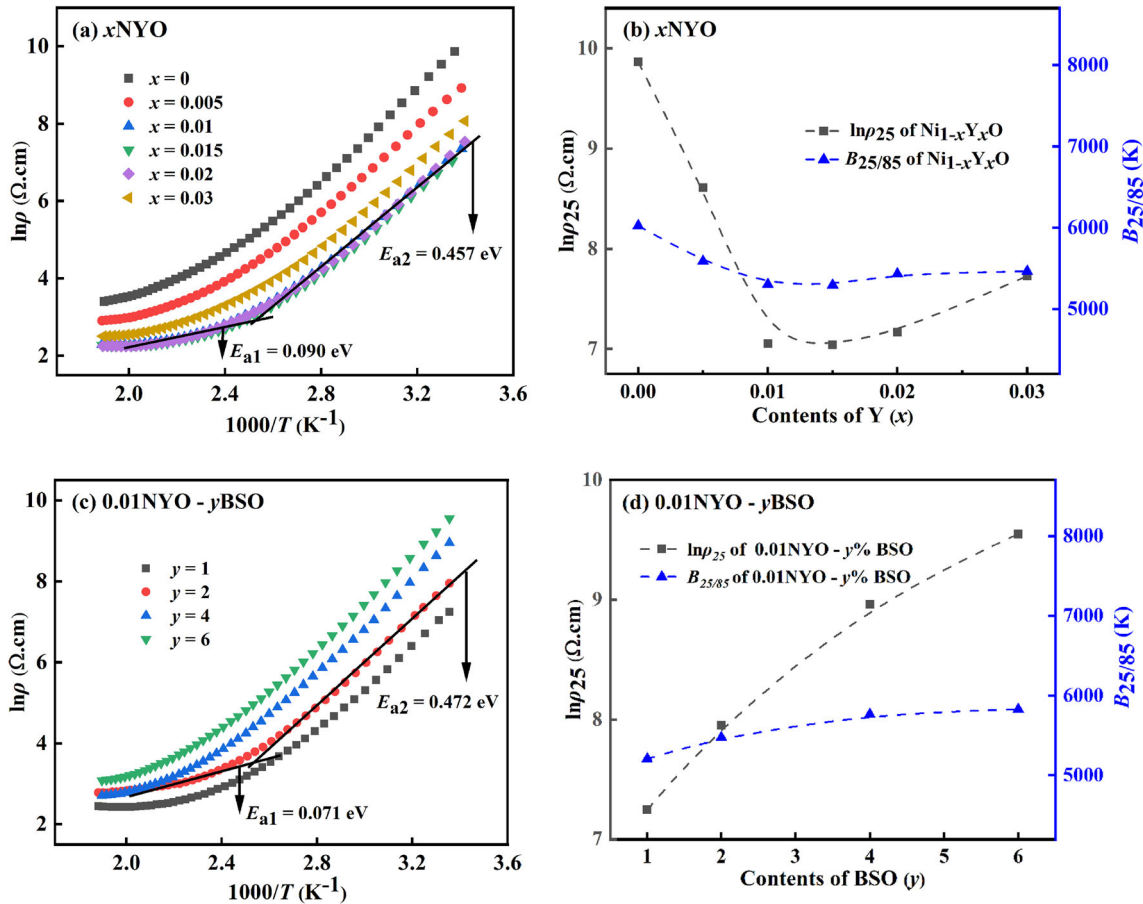
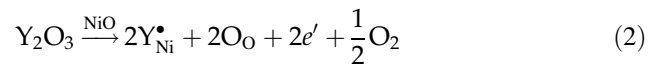


Fig. 6 Electrical properties of the studied NiO-based ceramics, **a** temperature dependence of resistivity of x NYO ceramics with various concentrations of Y^{3+} -ions, **b** Y^{3+} -ion concentration

sites, one weakly-bound electron forms. According to the band conduction mode in semiconductor, the weakly-bound electrons are easily activated and jump from donor level to conduction level, and then conductivity is promoted and resistivity reduces. In addition to band conduction mode, the so-called polaron hopping should also be an important conduction mode in transition metal oxide for the existence of different valences. For example, two sorts of nickel cations (Ni^{2+} and Ni^{3+}) might occur in NiO ceramic, so the polaron hopping of $Ni^{2+} + Ni^{3+} \leftrightarrow Ni^{3+} + Ni^{2+}$ can take place and plays role in conductivity of NiO based ceramics. These two conduction modes might contribute different role in different temperature regions, therefore a distinction of activation energies exist in the ceramics in different temperature regions.

dependence of ρ_{25} and $B_{25/85}$, **c** temperature dependence of resistivity of 0.01NYO– y BSO ceramics with various contents of BSO, **d** BSO content dependence of ρ_{25} and $B_{25/85}$



The B value is usually used to describe material sensitivity to temperature, and their definition is expressed by Eq. (3).

$$B = \frac{\ln \rho_{T1} - \ln \rho_{T2}}{1/T_1 - 1/T_2} \quad (3)$$

where, ρ_{T1} and ρ_{T2} represent resistivities at temperatures T_1 and T_2 , respectively. Generally, T_1 and T_2 are usually selected at 298 K (25 °C) and 358 K (85 °C), respectively. So the B value is often written as $B_{25/85}$. The calculated $B_{25/85}$ values of x NYO ceramics for various contents of Y^{3+} -ions are illustrated in Fig. 6b. The x NYO ceramics have high NTC $B_{25/85}$ values (> 5200 K).

Figure 6c shows the R – T relationship of 0.01NYO– y BSO ceramics with various BSO contents. BSO additives did not change the double conduction

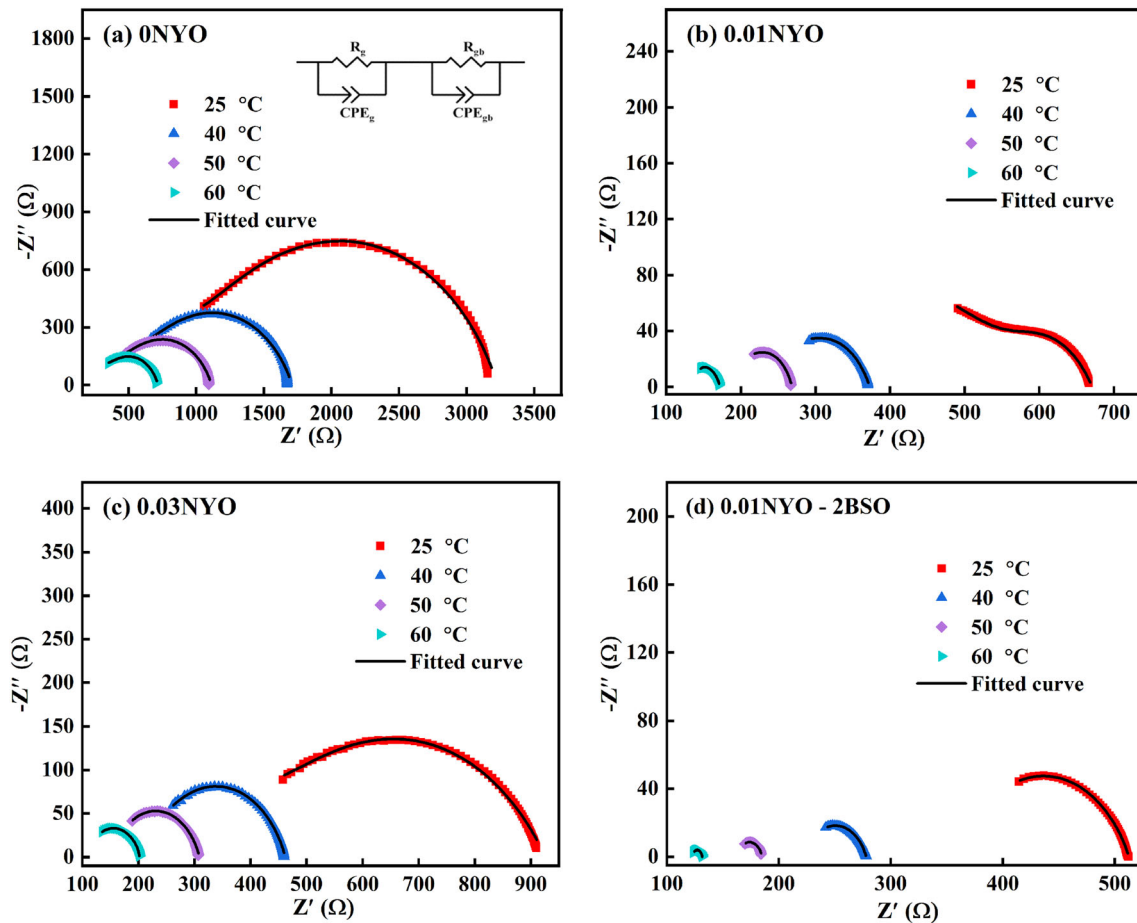


Fig. 7 Complex impedance spectra of ceramics at different temperatures, **a** 0NYO ceramic, the inset is an equivalent circuit for CIS fitting for all samples, **b** 0.01NYO ceramic, **c** 0.03NYO ceramic, **d** 0.01NYO–2BSO ceramic

Table 2 Comparison of results of CISs for various ceramics, room temperature resistances of grain effect (R_{g25}) and grain boundary effect (R_{gb25}) fitted from CISs in Fig. 7, conduction activation energy of grain effect ($E_{a(g)}$) and the grain boundary effect ($E_{a(gb)}$) obtained from Fig. 8

Sample	R_{g25} (Ω)	R_{gb25} (Ω)	$E_{a(g)}$ (eV)	$E_{a(gb)}$ (eV)
0NYO	1114.2	2117.4	0.270	0.437
0.01NYO	524.5	147.0	0.340	0.286
0.03NYO	468.7	457.9	0.359	0.381
0.01NYO–2BSO	360.1	152.5	0.264	0.692

mode of NTC feature as that x NYO ceramics. Figure 6d summarizes the variation of room temperature resistivity ρ_{25} and material constants $B_{25/85}$ of 0.01NYO– y BSO ceramics with the contents y of BSO. Both ρ_{25} and $B_{25/85}$ increase monotonically with the increase of y value.

As mentioned above, all the samples have high temperature sensitivity with $B_{25/85}$ larger than 5200 K, and the ρ_{25} values of NiO-based ceramics can be effectively adjusted by changing the contents of Y^{3+} -ions and/or BSO. The ρ_{25} ranges from 1143 to 19,188 Ω cm in present work. These should satisfy the requirements for various applications of NTC thermistors.

3.3 Impedance spectroscopy analysis

Complex impedance spectroscopy (CIS) is an important approach to characterize the electrical properties of ceramics. For an ideal polycrystalline material, a CIS is generally composed of three semi-circles corresponding to grain effect, grain boundary effect and electrode polarization effect, respectively. Figure 7 shows CISs of 0NYO, 0.01NYO, 0.03NYO and 0.01NYO–2BSO ceramics tested at different temperatures. Only one arc in each CIS can be

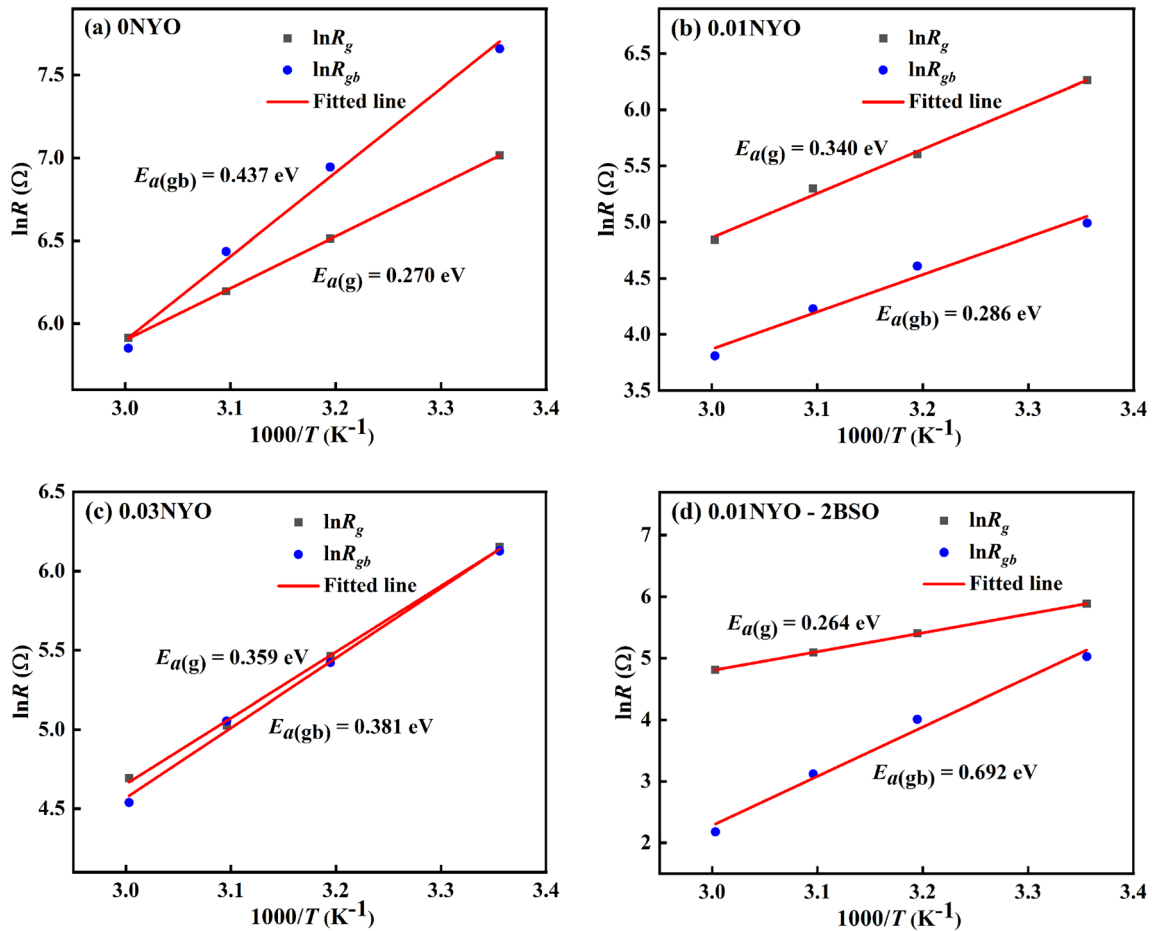


Fig. 8 Temperature dependence of resistances for grain effect and grain boundary effect of the studied NiO-based ceramics, **a** 0NYO, **b** 0.01NYO, **c** 0.03NYO, **d** 0.01NYO-2BSO

directly observed. An equivalent circuit composing of $(R_g - CPE_g)(R_{gb} - CPE_{gb})$ (see inset in Fig. 7a) was set up to reveal the conductive characteristics of each sample. Among them, R_g and R_{gb} represent the impedance from grain effect and grain boundary effect, respectively; CPE_g and CPE_{gb} are constant phase elements of grain effect and grain boundary effect, respectively, which are interpreted as the non-ideal Debye behavior of capacitor in a material. As shown in Fig. 7, the fitted curves (solid lines) are in good agreement with the measured data (scattered points). Some fitted results are listed in Table 2. It can be found that Y^{3+} dopant can significantly reduce both grain resistance and grain boundary resistance. The substitution of heterovalent cations can induce extra weakly bonded electrons for charge carriers (as described in Eq. (2)), increasing the conductivity of grain effect. On the other hand, the introduction of Y_2O_3 can enhance the ceramic sinter-ability (as see in

Fig. 2) and reduce the pores in ceramics. Thus, more compact grain boundaries reduce the boundary barrier.

Figure 8 shows the plots of R_g and R_{gb} in NiO-based ceramics changing with temperature, obtained by equivalent circuit fitting of CISs shown in Fig. 7. It can be seen that both R_g and R_{gb} decrease with increase of temperature, and show typical NTC characteristics. The $\ln R_{gb}$ of undoped NiO ceramic is larger than related $\ln R_g$ at each measurement temperature. While, all doped NiO ceramics, such as 0.01NYO, 0.03NYO or 0.01NYO-2BSO ceramics, present opposite results, i.e., $\ln R_g$ is larger than related $\ln R_{gb}$ at each measurement temperature. The activation energies of conduction of R_g and R_{gb} were calculated by Arrhenius equation, and the results are shown in Table 2. These indicate that the NTC effect of each NiO-based ceramic results from both grain effect and grain boundary effect.

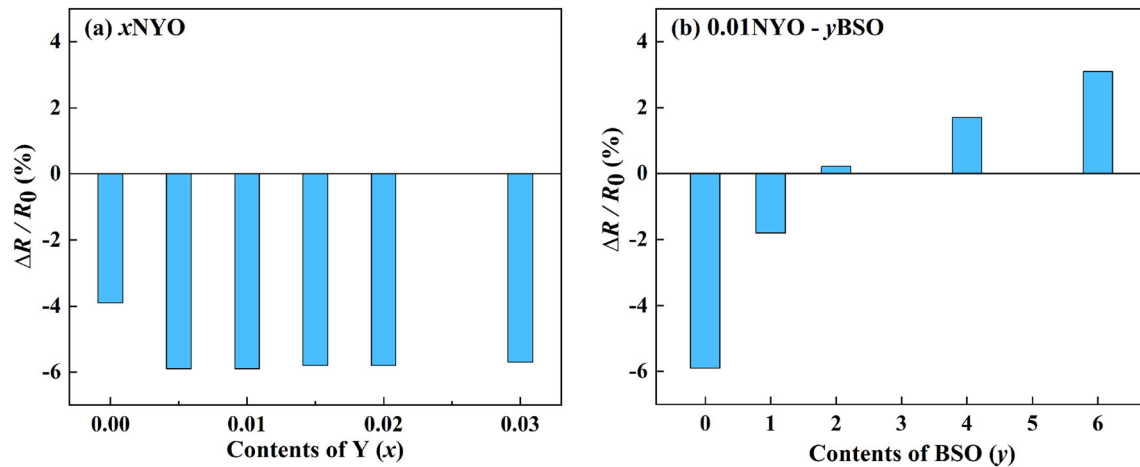


Fig. 9 Resistance change rates ($\Delta R/R_0$) of ceramics after aging treatment at 150 °C for 800 h, **a** x NYO ceramics, **b** 0.01NYO- y BSO ceramics

3.4 Aging performance

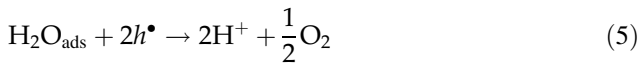
The resistance change rates ($\Delta R/R_0$) of x NYO ($x = 0, 0.005, 0.01, 0.015, 0.02, 0.03$) and 0.01NYO- y BSO ($y = 1, 2, 4, 6$) ceramics after having been aged at 150 °C for 800 h are shown in Fig. 9. The Y^{3+} -doped NiO (x NYO) ceramics have high $\Delta R/R_0$ and the resistance of each ceramic decreased after aging (see in Fig. 9a). The $\Delta R/R_0$ of undoped NiO ceramic is -3.9% and the maximum resistance change rate is -5.9% for 0.005NYO ceramic after aging 800 h. It is interesting that introduction of BSO could improve electrical stability of x NYO ceramics, as shown in Fig. 9b. The $\Delta R/R_0$ after 800 h aging are -1.8%, 0.21%, 1.7% and 3.1% for the 0.01NYO-1BSO, 0.01NYO-2BSO, 0.01NYO-4BSO, 0.01NYO-6BSO ceramics, respectively.

To further investigate the aging characteristics of NiO based NTC ceramics, X-ray photoelectron spectroscopy (XPS) was applied to analyze the valence variation of cations (Ni- and Sb-ions) in 0NYO, 0.01NYO and 0.01NYO-2BSO samples before and after aging treatment. The results are shown in Fig. 10. The XPS spectra have been calibrated using the binding energy of C 1s at 284.8 eV as reference. According to report of Lin et al. [25], the XPS spectrum of Ni $2p_{3/2}$ orbital could be comprised of six individual peaks. As shown in Fig. 10a-c, the peaks around 853 eV, 855 eV and 860 eV are attributed to Ni^{2+} , and the peaks around 856 eV, 857 eV and 863 eV are attributed to Ni^{3+} . Considering the overlap of peaks for O 1s and Sb $3d_{5/2}$ [26], here only Sb $3d_{3/2}$ spectra of 0.01NYO-2BSO ceramics are taken

into consideration. The results indicate that two characteristic peaks corresponding to Sb^{3+} and Sb^{5+} can be detected as shown in Fig. 10d.

The Ni $2p_{3/2}$ high-resolution spectra were fitted and analyzed by Gaussian Lorentz curves. As shown in Fig. 10a and b, the ratios of cationic contents between Ni^{2+} and Ni^{3+} (denoted as $[Ni^{2+}]/[Ni^{3+}]$) are 2.35:1 and 3.01:1 in 0NYO and 0.01NYO ceramics before aging, respectively. While, the $[Ni^{2+}]/[Ni^{3+}]$ values changed to 3.07:1 and 3.46:1 after aging treatment. This change indicates that redox reaction occurred during the aging process. As discussed in Fig. 6b and Eq. (2) for ceramic conductivity, the resistivity of x NYO ceramics is mainly influenced by the concentration of electrons in conduction band. The valence change of Ni ion is related to electron transfer in ceramics during aging. The aging treatment was carried out in ambient atmosphere, so moisture and oxygen might be easily adsorbed on the surface or at interfaces (grain boundaries) of ceramic. According to the report of Li et al. [15], during aging treatment, the adsorbed water (H_2O_{ads}) might capture electronic holes (h) from the surfaces and/or interfaces of x NYO ceramics and leads to reactions as shown in Eqs. (4) and (5) to form the $\cdot OH$ radicals, H^+ protons and O_2 molecules. As a result, the concentration of electronic holes in ceramics decreased. At the same time, the concentration of electron carriers increased for keeping electric neutrality. Therefore, the electrical conductivity of x NYO ceramics was enhanced. This is consistent with the results in Fig. 9a, i.e., ceramic resistances decreased. In the meanwhile, the excess electrons might also be

captured by Ni-ions, and then Ni³⁺ ions transformed to Ni²⁺ ions as shown in Eq. (6).



As shown in Fig. 10c and d, the concentration ratio of [Ni²⁺]/[Ni³⁺] in 0.01NYO–2BSO ceramic decreased slightly after aging, and changed from 3.10:1 to 3.04:1. However, the concentration ratio of [Sb³⁺]/[Sb⁵⁺] increased from 0.36:1 to 0.76:1, indicating that the concentration of Sb³⁺ ions increased or the one of Sb⁵⁺ decreased after aging. The third ionization energy of Ni is 3395 kJ mol⁻¹, and the

fourth and fifth ionization energies of Sb are 4260 and 5400 kJ mol⁻¹, respectively. These indicate that Sb⁵⁺ has a stronger ability to capture electrons than Ni³⁺. For the adsorption and reaction of H₂O_{ads} consumed holes as described in Eqs. (4) and (5), the excess electrons produced because the ceramic itself should be originally electrically neutral. The electrons could be captured by Sb-ion. So the influence of those electrons on Ni ions was significantly weakened and the [Ni²⁺]/[Ni³⁺] ratio changed slightly. These are consistent with the results of XPS analysis in Fig. 10. So according to the modes of band conduction and polaron hopping conduction, the slightly changed [Ni²⁺]/[Ni³⁺] ratio could not affect obviously the resistivity of the aged ceramics. The results show that BSO modification can improve the electrical stability

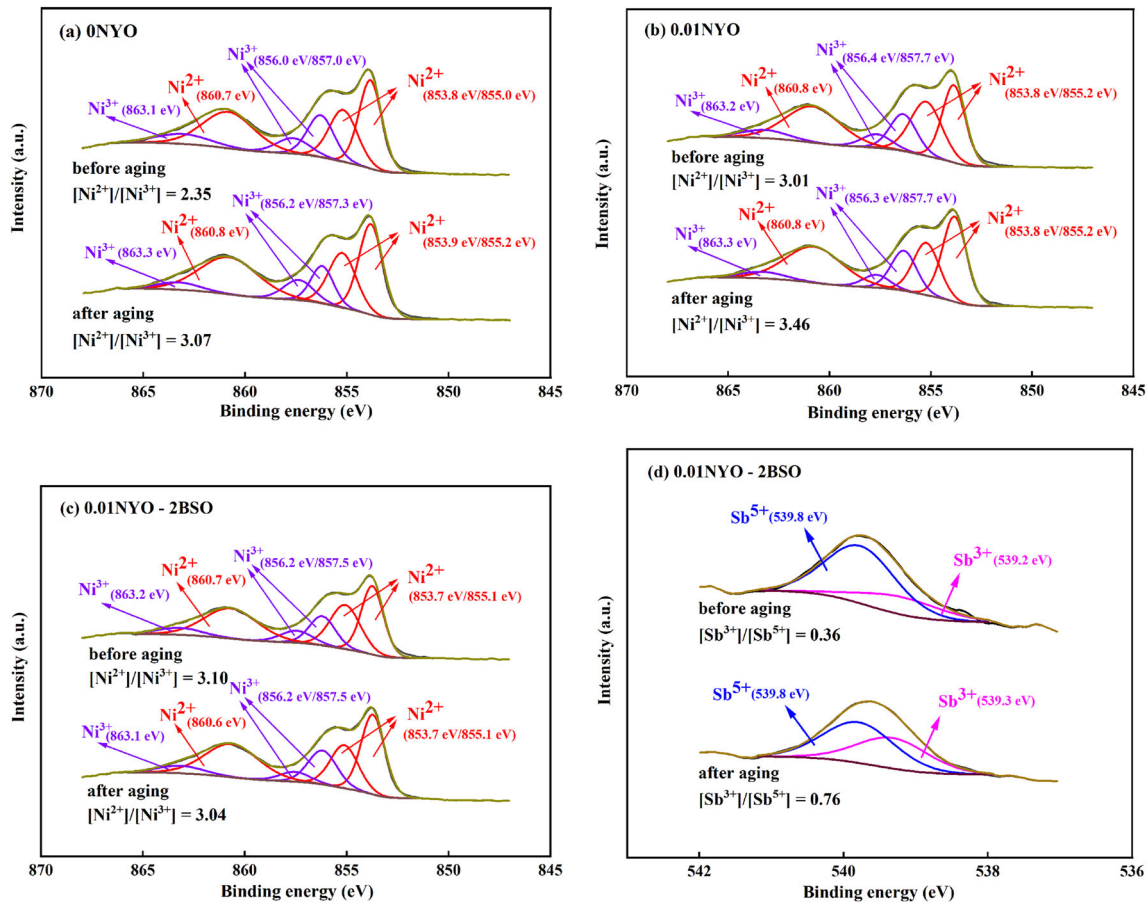


Fig. 10 XPS analysis of Ni- and Sb-ions in studied ceramics before and after aging, **a** Ni 2p_{3/2} orbitals of 0NYO ceramic, **b** Ni 2p_{3/2} orbitals of 0.01 NYO ceramic, **c** Ni 2p_{3/2} orbitals of 0.01NYO–2BSO ceramic, **d** Sb 3d_{3/2} orbitals of 0.01NYO–2BSO ceramic

of x NYO ceramics, and x NYO– y BSO meet the application requirements well when suitable content of BSO is selected.

4 Conclusions

Y^{3+} -doped NiO (x NYO) and Y_2O_3 /BiSbO₃ co-modified NiO ceramics possess typical NTC characteristic. Varying the concentrations of Y^{3+} -dopant and BiSbO₃ can effectively adjust room-temperature resistivity, and all ceramics have high temperature sensitivity with $B_{25/85}$ above 5200 K. Both grain effect and grain boundary effect contribute to the electrical conductivity and NTC feature. The introduction of BiSbO₃ can effectively improve the electrical stability, Y_2O_3 /BiSbO₃ co-modified NiO ceramic (0.01NYO–2BSO) have the lowest resistance change ratio of 0.21% after aging treatment at 150 °C in air for 800 h. For adjustable resistivity, high thermal sensitivity and electrical stability, the Y_2O_3 /BiSbO₃ co-modified NiO ceramics should have good potential for application as NTC thermistors.

Author contributions

ZL, HZ and DP contributed to the study conception and design. Material preparation, data collection and analysis were performed by DP, LH, CY and HW. The first draft of the manuscript was written by DP and all authors commented on previous versions of the manuscript. All authors read and approved the final manuscript.

Funding

This work is supported by the research funds from the National Natural Science Foundation of China (No. 51767021), Research and development program in key areas of Guangdong Province (No. 2019B090913002), Research and development project of Hunan Wedid Materials Technology Co., Ltd., China (No. 738010241).

Data availability

The datasets generated during and/or analyzed during the current study are available from the corresponding author on reasonable request.

Declarations

Competing interests The authors have no relevant financial or non-financial interests to disclose.

References

1. B. Li, Z. Li, S. Zhang, D. Peng, C. Gao, H. Zhang, Electrical properties of Ga/V-modified ZnO ceramic thermistors. *J. Mater. Sci. Mater. Electron.* **32**, 28792–28806 (2021)
2. B. Yang, Y. Feng, X. Deng, S. Ta, M. He, RuO₂ doping and its influence on phase structure, cations state, and electrical properties of Mn_{1.6}Co_{0.4}CuO₄ ceramics. *Ceram. Int.* **47**, 2107–2114 (2020)
3. M. Schubert, C. Münch, S. Schuurman, V. Poulain, R. Moos, Characterization of nickel manganite NTC thermistor films prepared by aerosol deposition at room temperature. *J. Eur. Ceram. Soc.* **38**, 613–619 (2018)
4. A. Feteira, Negative temperature coefficient resistance (NTCR) ceramic thermistors: an industrial perspective. *J. Am. Ceram. Soc.* **92**, 967–983 (2010)
5. P. Atanasijevic, P. Mihailovic, Temperature compensation of NTC thermistors based anemometer. *Sens. Actuator A Phys.* **285**, 210–215 (2019)
6. H. Han, K. Park, Y.-R. Hong, K. Shim, S. Mhin, Effect of Fe incorporation on cation distributions and hopping conduction in Ni-Mn-Co-O spinel oxides. *J. Alloys Compd.* **732**, 486–490 (2018)
7. C. Ma, H. Gao, TEM and electrical properties characterizations of Co_{0.98}Mn_{2.02}O₄ NTC ceramic. *J. Alloys Compd.* **749**, 853–858 (2018)
8. V.K. Haripriya, V.S. Sharon, K.A. Malini, Tailoring the properties of Ni-Mn based NTC thermistors by Cu and Li addition. *Phys Scr.* **96**, 125728 (2021)
9. W. Ren, N. Zhu, L. Li, H. Feng, Y. Wang, Y. Yang, Z. Yang, S. Shang, Improvement of aging issue in Zn_{0.4}Fe_{2.1}Co₂Mn_{1.5}O₈ thermistor films. *J. Eur. Ceram. Soc.* **39**, 4189–4193 (2019)
10. H. Li, H. Zhang, S. Thayil, A. Chang, X. Sang, X. Ma, Enhanced aging and thermal shock performance of Mn_{1.95-x}CO_{0.21}Ni_{0.84}Sr_xO₄ NTC ceramics. *J. Adv. Ceram.* **10**, 258–270 (2021)
11. J. Zhang, W. Kong, A. Chang, Fabrication and properties of high B value [Mn_{1.56}Co_{0.96}Ni_{0.48}O₄]_{1-x}[SrMnO₃]_x (0 ≤ x ≤

- 0.5) spinel–perovskite composite NTC films. *J. Mater. Sci. Mater. Electron.* **29**, 1–8 (2018)
12. B. Wang, J. Wang, D. Shang, A. Chang, J. Yao, Sintering temperature and XPS analysis of $\text{Co}_{2.77}\text{Mn}_{1.71}\text{Fe}_{1.10}\text{Zn}_{0.42}\text{O}_8$ NTC ceramics. *Mater. Chem. Phys.* **239**, 122098 (2020)
 13. H. Li, I.P.L. Thayil, X. Ma, X. Sang, H. Zhang, A. Chang, Electrical properties and aging behavior of Na-doped $\text{Mn}_{1.95}\text{Co}_{0.21}\text{Ni}_{0.84}\text{O}_4$ NTC ceramics. *Ceram. Int.* **46**, 24365–24370 (2020)
 14. Z. Yang, H. Zhang, Z. He, B. Li, Z. Li, Influence of B^{3+} - and Na^+ -ions on electrical property and temperature sensitivity of NiO-based ceramics. *J. Mater. Sci. Mater. Electron.* **30**, 3088–3097 (2019)
 15. B. Li, Z. Li, D. Peng, L. Huang, S. Zhang, H. Zhang, Sb-doped ZnO ceramics: NTC thermistors with high temperature sensitivity and electrical stability. *J. Mater. Sci. Mater. Electron.* **32**, 24296–24307 (2021)
 16. G. Jiang, Z. Li, C. You, W. Hao, H. Zhang, Temperature sensitivity and electrical stability of Sb/Mn co-doped SnO_2 ceramics. *J. Mater. Sci. Mater. Electron.* **32**, 16945–16955 (2021)
 17. C. You, Z. Li, S. Zhang, G. Jiang, H. Zhang, Electrical properties of Sr-modified CuO ceramics. *J. Mater. Sci. Mater. Electron.* **32**, 15907–15916 (2021)
 18. X. Sun, S. Leng, H. Zhang, Z. He, Z. Li, Electrical properties and temperature sensitivity of Li/Mg modified $\text{Ni}_{0.7}\text{Zn}_{0.3}\text{O}$ based ceramics. *J. Alloys Compd.* **763**, 975–982 (2018)
 19. P. Ouyang, H. Zhang, Y. Zhang, J. Wang, Z. Li, Zr-substituted SnO_2 -based NTC thermistors with wide application temperature range and high property stability. *J. Mater. Sci. Mater. Electron.* **26**, 6163–6169 (2015)
 20. H. Zhang, T. Liu, L. Zhao, H. Jiang, A. Chang, Effect of Al_2O_3 addition on the microstructure and electrical properties of LaMnO_3 -based NTC thermistors. *J. Mater. Sci. Mater. Electron.* **28**, 14195–14201 (2017)
 21. T. Battault, R. Legros, A. Rousset, Aging of iron manganite negative temperature coefficient thermistors. *J. Mater. Res.* **13**, 1238–1242 (1998)
 22. F. Guan, Z. Dang, S. Huang, J. Wang, Y. Wu, $\text{LaCr}_{1-x}\text{Fe}_x\text{O}_3$ ($0 \leq x \leq 0.7$): a novel NTC ceramic with high stability. *J. Eur. Ceram. Soc.* **40**, 5597–5601 (2020)
 23. C. Ma, Y. Liu, Y. Lu, H. Gao, H. Qian, J. Ding, Effect of Zn substitution on the phase, microstructure and electrical properties of $\text{Ni}_{0.6}\text{Cu}_{0.5}\text{Zn}_x\text{Mn}_{1.9-x}\text{O}_4$ ($0 \leq x \leq 1$) NTC ceramics. *Mater. Sci. Eng. B.* **188**, 66–71 (2014)
 24. C. Gao, Z. Li, L. Yang, D. Peng, H. Zhang, Investigation of electrical and aging properties of Bi-modified $(\text{Zn}_{0.4}\text{Ni}_{0.6})_{1-x}\text{Na}_x\text{O}$ ceramic thermistors. *J. Eur. Ceram. Soc.* **41**, 4160–4166 (2021)
 25. T.J. Lin, X. Meng, L. Shi, Catalytic hydrocarboxylation of acetylene to acrylic acid using Ni_2O_3 and cupric bromide as combined catalysts. *J. Mol. Catal. A Chem.* **396**, 77–83 (2015)
 26. A. Barbaro, S. Larrondo, S. Duhalde, N. Amadeo, Effect of titanium-doping on the properties of vanadium antimonate catalysts. *Appl. Catal. A Gen.* **193**, 277–283 (2000)

Publisher's Note Springer Nature remains neutral with regard to jurisdictional claims in published maps and institutional affiliations.